

FOTOC complexity in an extended Lipkin-Meshkov-Glick model

Nitesh Jaiswal,^{*} Mamta Gautam,[†] Ankit Gill,[‡] and Tapobrata Sarkar[§]
Department of Physics, Indian Institute of Technology Kanpur-208016, India

We study fidelity out-of-time-order correlators (FOTOCs) in an extended Lipkin-Meshkov-Glick model and demonstrate that these exhibit distinctive behaviour at quantum phase transitions in both the ground and the excited states. We show that the dynamics of the FOTOC have different behaviour in the symmetric and broken-symmetry phases, and as one approaches phase transition. If we rescale the FOTOC operator with time, then for small times, we establish that it is identical to the Loschmidt echo. We also compute the Nielsen complexity of the FOTOC operator in both phases, and apply this operator on the ground and excited states to obtain the quasi-scrambled state of the model. The FOTOC operator introduces a small perturbation on the original ground and excited states. For this perturbed state, we compute the quantum information metric to first order in perturbation, in the thermodynamic limit. We find that the associated Ricci scalar diverges at the phase transition on the broken-symmetry phase side, in contrast to the zeroth order result. Finally, we comment upon the Fubini-Study complexity in this model.

I. INTRODUCTION

Out-of-time-order correlators (OTOCs) were originally introduced in the context of vertex corrections in superconductors [1] and currently find widespread usage as a measure of quantum chaos, with its growth rate being related to the Lyapunov exponent [2–5]. The OTOC is also the key quantity in studies of quantum information geometry (QIG), in particular in quantum information scrambling [6–8] and quantum phase transitions (QPTs) [9–15]. Depending on how the OTOC is computed, it may be referred to as the microcanonical OTOC, the fidelity OTOC (FOTOC), the thermal OTOC, etc. In quantum systems, the OTOC may serve as a diagnostic tool to probe ground-state QPTs (GSQPTs) and excited-state QPTs (ESQPTs). Another reason why the FOTOC is important is that the OTOC features exponential growth at unstable points or in chaotic regions of the quantum system. However, exact numerical treatment is only possible for a small system size N , as many-body observables quickly saturate with time, $t \sim \log N$. This limitation can be overcome if one uses the FOTOC [16, 17]. One purpose of this paper is to examine the FOTOC as a probe for QPTs in QIG, as it can be directly implemented and measured in experiments with trapped ions [17, 18]. The detailed experimental studies and demonstrations to measure OTOCs are performed in [19–22].

On the other hand, scrambling is the process by which information stored in local degrees of freedom is dispersed across a large number of degrees of freedom. The Heisenberg picture, in which quantum operators evolve and quantum states are stationary, contains a precise formulation of quantum scrambling. The structure of the

time-dependent Heisenberg operator $\hat{W}(t)$ for any operator \hat{W} resembles a classical butterfly effect. Even if \hat{W} is a local operator, such as a spin operator at a given site, $\hat{W}(t)$ will eventually spread across many sites, making it inaccessible to local measures [17, 23–25]. There are two distinct types of scramblings known in the current literature [26, 27], which are termed as *genuine scrambling*, where a localised initial operator in phase space spreads significantly, and *quasi-scrambling*, where a localised initial operator stays localised, but can nonetheless move around in phase space. Even if quasi-scramblers are not fully spread operators, useful insights into genuine scrambling can be obtained by their study. A second purpose of this paper is to study the QIG of quasi-scrambled states.

Indeed, the primary reason for using FOTOC is that it allows us to visualize the dynamics of scrambling using a semi-classical picture. The FOTOC can be mapped to a two-point correlator, allowing us to compute it in a parameter regime inaccessible to exact numerical diagonalisation using phase-space methods. Secondly, the FOTOC has the potential to shed light on QPTs. FOTOC's time evolution have distinct behaviours in different phases, whereas its behaviour on QPTs is very different in comparison to these phases. Unlike microcanonical OTOCs, where we need to choose order parameters as our operators to identify the existence of QPTs, for FOTOCs we just need to select the Hermitian operator.

With these motivations to study the above mentioned information theoretic quantities, in this paper we consider an extension of the Lipkin-Meshkov-Glick model which we call the eLMG model, introduced in [28], which is attractive, as it allows very efficient analytical calculations and numerical treatments much like the original LMG model. The LMG model which is exactly solvable, was introduced in the context of nuclear physics [29], and is an ideal arena to explore effects of long range interactions (beyond the nearest neighbour ones which are well studied for example in the transverse field XY model) which result in quantum phase transitions in the ther-

^{*} nitesh@iitk.ac.in

[†] mamtag@iitk.ac.in

[‡] ankitgill20@iitk.ac.in

[§] tapo@iitk.ac.in

modynamic limit [30],[31]. In the context of the eLMG model as well, analytical calculations are simplified, since the model reduces to a simple harmonic oscillator after a Bogoliubov transformation. The numerical calculations too are straightforward here, since the size of the Hamiltonian matrix to be diagonalised grows linearly with the number of spins N , if we consider the maximum spin sector $j = N/2$, which contains low energy states. The eLMG model is considered here rather than the standard LMG model, since it was shown in [32] that information geometry is ill-defined in the latter. In contrast, QIG is well defined in the eLMG model.

In this work, we find the Nielsen complexity (NC) [33–43] of the time-dependent FOTOC operator $\hat{W}(t)$ in an eLMG model, and will show that the derivative of the NC diverges, if we approach the QPT line from the broken-symmetry phase side. We also apply the time-dependent FOTOC operator on the ground and excited state to get the quasi-scrambled state. We then compute the quantum information metric (QIM) [40–44] for these quasi-scrambled states and study its various properties. Natural units with $\hbar = 1$ are used throughout.

II. THE HAMILTONIAN AND ITS SEMICLASSICAL DESCRIPTION

We now briefly review some of the necessary formalism of [28]. The Hamiltonian of an eLMG model is

$$H = \Omega \hat{J}_z + \Omega_x \hat{J}_x + \frac{\xi_y}{j} \hat{J}_y^2, \quad (1)$$

where $\hat{J}_\alpha = \sum_{i=1}^N \sigma_\alpha^i$ are the collective pseudospin operators, and σ_α^i are the Pauli spin operators for a particular two-level system i along $\alpha = x, y, z$ directions. The parameter Ω gives the energy difference for the two-level system, and from now on we will set $\Omega = 1$. The parameter space of interest is $\Omega_x, \xi_y \in \mathbb{R}$, where Ω_x is the strength of the linear term included in the LMG model to transform it to the eLMG model and ξ_y is the coupling strength. The collective spin operators follow the commutation relation $[\hat{J}_\alpha, \hat{J}_\beta] = i\epsilon_{\alpha\beta\gamma} \hat{J}_\gamma$, and the magnitude of total spin operator is conserved, i.e., $[H, \hat{J}^2] = 0$, with $j(j+1)$ being the eigenvalue of \hat{J}^2 . The j in the denominator of Eq. (1) ensures finite energy per spin in the thermodynamic limit, and as mentioned in the introduction, here for simplicity, we consider the maximum spin sector by fixing $j = N/2$ to get the size of the system. The classical eLMG Hamiltonian is obtained by taking its expectation value with respect to Bloch coherent states $|z\rangle = (1 + |z|^2)^{-j} e^{z\hat{J}_+} |j, -j\rangle$. Here, \hat{J}_+ is the raising operator, and $|j, -j\rangle$ is the state with the lowest pseudospin projection, and $z \in \mathbb{C}$ is defined in terms of spherical polar coordinates, $z = \tan\left(\frac{\theta}{2}\right) e^{-i\phi}$ with semiclassical polarisation,

$$\langle \hat{J} \rangle = j (\sin \theta \cos \phi, \sin \theta \sin \phi, \cos \theta). \quad (2)$$

The classical eLMG Hamiltonian has the form

$$h = -\cos \theta + \Omega_x \sin \theta \cos \phi + \xi_y \sin^2 \theta \sin^2 \phi, \quad (3)$$

which can also be written using convenient canonical variables Q and P , defined as

$$Q = \sqrt{2(1 - \cos \theta)} \cos \phi, \quad P = -\sqrt{2(1 - \cos \theta)} \sin \phi. \quad (4)$$

With the classical Hamiltonian, we can obtain the stationary points of the eLMG model, which corresponds to vanishing velocities

$$\dot{Q} = \frac{\partial h}{\partial P} = 0, \quad \dot{P} = -\frac{\partial h}{\partial Q} = 0, \quad (5)$$

in the region $0 \leq \theta \leq \pi$ and $0 \leq \phi \leq 2\pi$. The stationary points under these conditions are

$$\begin{aligned} (\theta_1, \phi_1) &= \left(\arccos \left(\frac{1}{\sqrt{\Omega_x^2 + 1}} \right), 0 \right), \\ (\theta_2, \phi_2) &= \left(\arccos \left(\frac{1}{\sqrt{\Omega_x^2 + 1}} \right), \pi \right). \end{aligned} \quad (6)$$

Another stationary point (θ_3, ϕ_3) that was given in [28] is only valid for $\xi_y \leq -\sqrt{1 + \Omega_x^2}/2$. In what follows, we consider the domain $\xi_y \geq 0$, and will only illustrate the results for $\xi_y \leq 0$ whenever necessary. Finally, the stationary point

$$(\theta_4, \phi_4) = \left(\arccos \left(-\frac{1}{2\xi_y} \right), \arccos \left(\frac{\Omega_x}{\sqrt{4\xi_y^2 - 1}} \right) \right), \quad (7)$$

is valid for $\xi_y \geq \sqrt{1 + \Omega_x^2}/2$.

The energies $e_n = h(\theta_n, \phi_n)$ associated with the stationary points are $e_{1,2} = \pm\sqrt{1 + \Omega_x^2}$, and $e_3 = e_4 = (1 + \Omega_x^2)/(4\xi_y) + \xi_y$. Note that the energies e_3 and e_4 are defined only in the regions $\xi_y \leq -\sqrt{1 + \Omega_x^2}/2$ and $\xi_y \geq \sqrt{1 + \Omega_x^2}/2$, respectively, as follows from our previous discussion. The GSQPT line, defined as $\xi_y = -\sqrt{1 + \Omega_x^2}/2$, separates the two quantum phases of the ground state, described on one side by (θ_2, ϕ_2) and on the other by (θ_4, ϕ_4) coherent states. Similarly, the ESQPT line, denoted by $\xi_y = \sqrt{1 + \Omega_x^2}/2$, acts as a dividing line between the quantum phases of the excited state described by coherent states $(\theta_{1,4}, \phi_{1,4})$ on the two sides.

III. FOTOC AND QUANTUM PHASE TRANSITIONS

We now examine the GSQPT and ESQPT of an eLMG model using FOTOCs. Typical usage identifies the

OTOCs as measures of the dynamics of quantum information scrambling. Concurrently, OTOCs are defined as $F(t) = \langle \hat{W}^\dagger(t) \hat{V}^\dagger \hat{W}(t) \hat{V} \rangle$, where \hat{V} and \hat{W} are two Hermitian operators, $\hat{W}(t) = e^{i\hat{H}t} \hat{W} e^{-i\hat{H}t}$ is the time-dependent operators at time t in the Heisenberg representation, with \hat{H} being the Hamiltonian of the system, and $\langle \dots \rangle$ represents thermal averaging. This OTOC is called FOTOC [16, 17] if we only allow a small perturbation $\varepsilon \ll 1$ to the operator $\hat{W} = e^{i\varepsilon \hat{G}}$, where \hat{G} is a Hermitian operator and sets $\hat{V} = |\psi_{in}\rangle \langle \psi_{in}|$ to be a projection operator onto an initial state $|\psi_{in}\rangle$. Then for the pure state, $F(t) \equiv |\langle \psi_{in} | \hat{W}(t) | \psi_{in} \rangle|^2$ is known as FOTOC and up to $\mathcal{O}(\varepsilon^2)$, it reduces to $F_G(t) \approx 1 - \varepsilon^2 \sigma_G^2(t)$ where

$$\sigma_G^2(t) = \left(\langle \psi_{in} | \hat{G}^2(t) | \psi_{in} \rangle - \langle \psi_{in} | \hat{G}(t) | \psi_{in} \rangle^2 \right). \quad (8)$$

This last relation directly links the FOTOC and the two-point correlator. This also maps it to the variances of the operator $\hat{G}(t)$, i.e., the FOTOC can be viewed as the square of the uncertainty in the operator $\hat{G}(t)$ in the initial state up to order ε^2 . In our generic treatment to compute the FOTOC, we choose the operator $\hat{G} = \hat{Q}, \hat{P}$, which are position and momentum operators respectively of the form

$$\hat{Q} = \frac{1}{\sqrt{2}}(\hat{a} + \hat{a}^\dagger), \quad \hat{P} = \frac{i}{\sqrt{2}}(\hat{a}^\dagger - \hat{a}), \quad (9)$$

and $\hat{V} = |z\rangle \langle z|$, which is a projection operator on the spin coherent state. By selecting the position and momentum operators, the FOTOC measures the spread of the wavepacket's size, depicting quantum evolution of the phase space dynamics. Since the wavepacket can spread in either way in phase space, we must examine the growth of $F_Q(t) + F_P(t)$. Note that in order to operate \hat{a} and \hat{a}^\dagger on spin coherent states, we first write them in terms of $\hat{J}_\pm = \hat{J}_x \pm i\hat{J}_y$: $\hat{a} = \hat{J}_- / \sqrt{2j}$ and $\hat{a}^\dagger = \hat{J}_+ / \sqrt{2j}$.

In Fig. (1), we have presented the numerical results of the FOTOC evaluated for an eLMG model. The time evolution of the real part of the FOTOC computed for the symmetric phase (θ_1, ϕ_1) , $\xi_y = 1$ in Fig. 1(a), broken-symmetry phase (θ_4, ϕ_4) , $\xi_y = 3$, in Fig. 1(b), with $j = 400$, and $\Omega_x = 4$ has been shown here. As shown in Fig. 1(a), the evolution of the FOTOC in the symmetric phase consists of a sequence of typical wave packets. The envelope of a wave packet is a measure of the variance of the sum of the position and momentum operators, which extends over a finite time. The pattern of the wave packet remains the same, even for a long time, as we have checked for time values up to 5000. In contrast with the symmetric phase, the time evolution of the FOTOC in the broken-symmetry phase consists of a series of continuous oscillations with a mixture of small and large amplitudes. The oscillations persist here for large times as well. In Fig. (2), we plot the evolution of the FOTOC on the QPT line $\xi_y = \sqrt{1 + \Omega_x^2}/2$, where, after a rapid increase, the FOTOC begins oscillating with

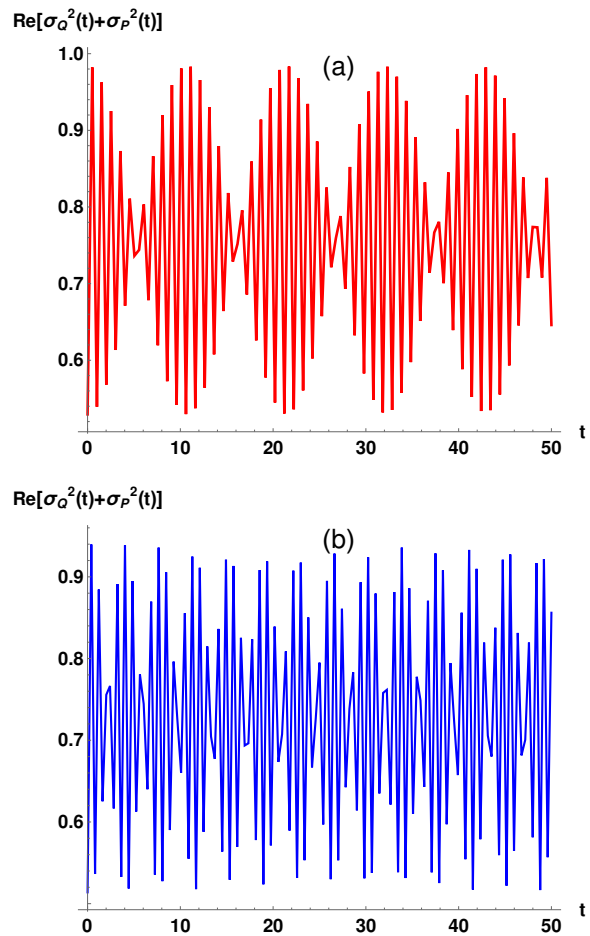


FIG. 1: Comparison between the behavior of the FOTOC's real part versus time in the symmetric phase (θ_1, ϕ_1) , $\xi_y = 1$ (a), and broken-symmetry phase (θ_4, ϕ_4) , $\xi_y = 3$ (b), with $j = 400$ and $\Omega_x = 4$ of the excited state. The difference in the oscillatory nature of the two phases is apparent from the top and bottom panel.

an irregular pattern of high amplitude. These oscillations do not die out with time even at QPTs, contrary to the microcanonical OTOC's in [10, 12]. In conclusion, the ESQPT is characterised by the FOTOC's abrupt increase in amplitude and irregular oscillations, while the oscillatory patterns in the two phases are very distinct.

It is worth noting that a similar situation arises for the GSQPT. We have repeated the analysis above for the ground state, and find that GSQPT occurs at $\xi_y = -\sqrt{1 + \Omega_x^2}/2$, as evidenced by an increase in amplitude with irregular oscillations. One phase of the ground state is described by (θ_2, ϕ_2) for $\xi_y > -\sqrt{1 + \Omega_x^2}/2$ and this has the FOTOC's temporal evolution similar to what we found for the symmetric phase of the ESQPT. The other phase is described by (θ_4, ϕ_4) , the analysis of which was done in the excited state case. In addition, the FOTOC also provides a link between the classical and quantum

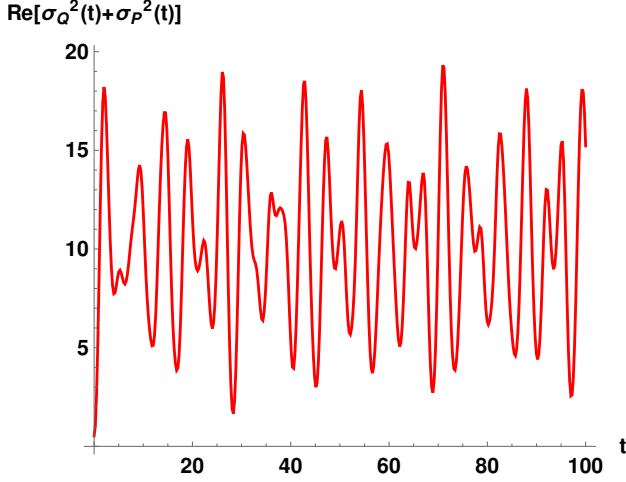


FIG. 2: The temporal evolution of the FOTOC at ESQPT is described by $\xi_y = \sqrt{1 + \Omega_x^2}/2$ with $j = 40$ and $\Omega_x = 4$. The oscillations are irregular, with much higher amplitudes as compared to symmetric and broken-symmetry phases.

Lyapunov exponents [16, 17]. The eLMG model has unstable points (θ_1, ϕ_1) for $\xi_y > \sqrt{1 + \Omega_x^2}/2$ and (θ_2, ϕ_2) for $\xi_y < -\sqrt{1 + \Omega_x^2}/2$. This gives rise to a positive classical Lyapunov exponent given by

$$\lambda_{cl} = \sqrt{\sqrt{1 + \Omega_x^2}(2\xi_y - \sqrt{1 + \Omega_x^2})}, \quad (10)$$

where the FOTOC exhibits exponential growth, i.e., $1 - \text{Re}[F_G(t)] \sim e^{\lambda_Q t}$. Here, λ_Q is the quantum Lyapunov exponent and we have checked numerically that $\lambda_Q \simeq 2\lambda_{cl}$.

A. Loschmidt Echo and the FOTOC

The LE, denoted by \mathcal{L} (see, e.g. [41]), quantifies how similar a state is to one that has been time-evolved by a Hamiltonian \hat{H}_F and then backward in time by a slightly different Hamiltonian \hat{H} . We will take the state to be the spin coherent state, the Hamiltonian $\hat{H} = H$ and $\hat{H}_F = H - \varepsilon\hat{G}$, then

$$\mathcal{L} = |\langle z | e^{iHt} e^{-i(H-\varepsilon\hat{G})t} | z \rangle|^2, \quad (11)$$

By using the Zassenhaus formula $e^{t(\hat{X}+\hat{Y})} = e^{t\hat{X}} e^{t\hat{Y}} e^{-\frac{t^2}{2}[\hat{X},\hat{Y}]} \dots$, where \hat{X} and \hat{Y} are any operators, we can expand $e^{-it(H-\varepsilon\hat{G})}$ to rewrite the above expression of LE as

$$\mathcal{L} = |\langle z | e^{iHt} e^{i\varepsilon\hat{G}t} e^{-iHt} e^{-\frac{\varepsilon^2 t^2}{2}[\hat{G},H]} \dots | z \rangle|^2. \quad (12)$$

Finally, if we rescale the operator \hat{G} in the FOTOC expression with time as $\hat{G} \rightarrow \hat{G}t$, we have a simple relation

between the LE and the FOTOC expressions for small times,

$$F(\hat{G} \rightarrow \hat{G}t, t) = \mathcal{L} + \frac{\varepsilon t^2}{2} \langle z | \left([\hat{G}, H] + [\hat{G}, H]^\dagger \right) | z \rangle + \mathcal{O}(t^3). \quad (13)$$

By choosing $\hat{G} = \hat{J}_x$ Eq. (13) takes the form

$$F(\hat{J}_x \rightarrow \hat{J}_x t, t) = \mathcal{L} + \mathcal{O}(t^3), \quad (14)$$

which we have also checked numerically for time $t = 0.1$. In a previous analysis of the transverse XY model [41], we had established an exponential relation between the LE and the NC. Interestingly we find a linear relation here instead between the LE and the FOTOC operator.

IV. NC OF THE FOTOC OPERATOR

The FOTOC we mentioned in earlier sections can be seen as the overlap of two states, and can be defined through the following process : starting from the spin coherent state $|z\rangle$, the first state is created by applying $\hat{V} = |z\rangle\langle z|$, evolving for time t , then applying $\hat{W} = e^{i\varepsilon\hat{Q}}$, and then evolving for time $-t$ to get $|\psi_1(t)\rangle = e^{i\hat{H}t} e^{i\varepsilon\hat{Q}} e^{-i\hat{H}t} |z\rangle$. Similarly, the second state is produced by evolving $|z\rangle$ for time t , then applying \hat{W} , evolving for time $-t$, and then applying \hat{V} to get $|\psi_2(t)\rangle = |z\rangle\langle z| e^{i\hat{H}t} e^{i\varepsilon\hat{Q}} e^{-i\hat{H}t} |z\rangle$. The FOTOC is the quantum overlap of these two states, i.e., $F(t) = \langle \psi_2(t) | \psi_1(t) \rangle$. The $e^{i\varepsilon\hat{Q}}$ operator will henceforth be referred to as the FOTOC operator and we will compute the NC corresponding to the time evolved FOTOC operator. We first evolve it with the Hamiltonians of the symmetric and the broken-symmetry phase of the excited state of the eLMG model. The Hamiltonians of the symmetric phase, \hat{H}_s and broken-symmetry phase, \hat{H}_b are [28]

$$\hat{H}_s \simeq j\sqrt{1 + \Omega_x^2} - \left(\frac{\sqrt{1 + \Omega_x^2} - 2\xi_y}{2} \right) \hat{p}^2 - \frac{\sqrt{1 + \Omega_x^2}}{2} \hat{Q}^2, \quad (15)$$

and

$$\begin{aligned} \hat{H}_b \simeq & j \frac{4\xi_y^2 + \Omega_x^2 + 1}{4\xi_y} - \frac{\xi_y (4\xi_y^2 - \Omega_x^2 - 1)}{4\xi_y^2 - 1} \hat{p}^2 \\ & + \frac{\Omega_x \sqrt{4\xi_y^2 - \Omega_x^2} - 1}{2(4\xi_y^2 - 1)} \left(\hat{Q}\hat{p} + \hat{p}\hat{Q} \right) \\ & - \frac{16\xi_y^4 - 8\xi_y^2 + \Omega_x^2 + 1}{4\xi_y (4\xi_y^2 - 1)} \hat{Q}^2, \end{aligned} \quad (16)$$

respectively, which describe harmonic oscillators with frequencies $\omega_s = (1 + \Omega_x^2)^{1/4} \sqrt{\Gamma_-}$ for the symmetric phase and $\omega_b = \sqrt{4\xi_y^2 - \Omega_x^2} - 1$ for the broken-symmetry phase, and also $\Gamma_- = \sqrt{1 + \Omega_x^2} - 2\xi_y$. The

time-dependent FOTOC operator evolved by $\hat{H}_{s,b}$ is $\hat{W}_{s,b}(t) = e^{i\hat{H}_{s,b}t} e^{i\varepsilon\hat{Q}} e^{-i\hat{H}_{s,b}t}$, and can be solved exactly using an extended version of Hadamard Lemma [26] : $e^{\hat{A}} f(\hat{B}) e^{-\hat{A}} = f(\hat{B}')$, where \hat{A} and \hat{B} are any operators, and $f(\hat{B}')$ is any function with

$$\hat{B}' = \hat{B} + [\hat{A}, \hat{B}] + \frac{1}{2!}[\hat{A}, [\hat{A}, \hat{B}]] + \dots \quad (17)$$

Plugging $\hat{A} = i\hat{H}_{s,b}t$ and $\hat{B} = \hat{Q}$ in the above Eq. (17), we can get the exact form of the expressions of time-dependent FOTOC operators, i.e., $\hat{W}_{s,b}(t) = e^{i\varepsilon\hat{Q}_{s,b}(t)}$, where $\hat{Q}_{s,b}(t) = \hat{Q}\mathcal{F}_{s,b}(t) + \hat{P}\mathcal{G}_{s,b}(t)$, with

$$\begin{aligned} \mathcal{F}_s(t) &= \cos \omega_s t, & \mathcal{G}_s(t) &= -\frac{\sqrt{\Gamma_-}}{(1 + \Omega_x^2)^{1/4}} \sin \omega_s t, \\ \mathcal{F}_b(t) &= \cos \omega_b t + \frac{\Omega_x \sin \omega_b t}{4\xi_y^2 - 1}, & \mathcal{G}_b(t) &= -\frac{2\xi_y \omega_b \sin \omega_b t}{4\xi_y^2 - 1}. \end{aligned} \quad (18)$$

Now, $\hat{W}_{s,b}(t)$ are the elements, and $\{i\hat{Q}, i\hat{P}, -i\mathbb{1}\}$ are the generators of the Heisenberg group, whose algebra is defined as follows

$$[i\hat{Q}, i\hat{P}] = -i\mathbb{1}, \quad [i\hat{Q}, -i\mathbb{1}] = 0, \quad [i\hat{P}, -i\mathbb{1}] = 0. \quad (19)$$

The detailed calculation of computing the NC of the time-dependent FOTOC operators can be found in Appendix A, and the final expression takes the form

$$C_{s,b}(t) = \varepsilon^2 (\mathcal{F}_{s,b}^2(t) + \mathcal{G}_{s,b}^2(t)). \quad (20)$$

To clarify the relationship between the NC of the time-

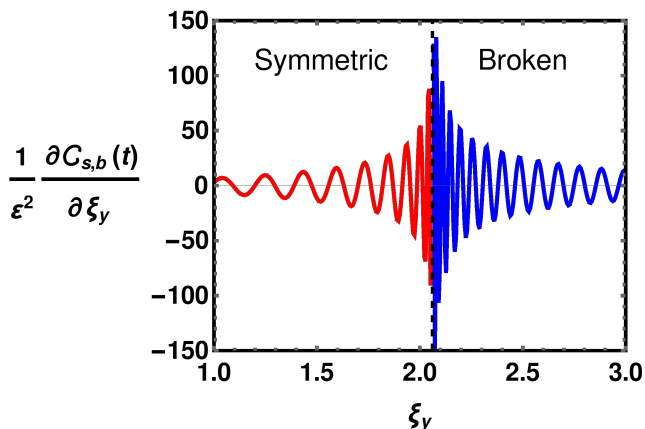


FIG. 3: The derivative of NC of the time-dependent FOTOC operator in the symmetric (solid red) and broken-symmetry (solid blue) phase for $\Omega_x = 4$ and $t = 10$.

dependent FOTOC operator and the QPT, we first examine the dynamical behaviour of the derivative of the NC with respect to ξ_y , and this is shown in Fig. (3)

for $\Omega_x = 4$ and $t = 10$. The derivative of the NC in the symmetric phase, $\partial C_s(t)/\partial \xi_y$ shows sinusoidal behaviour, and the amplitude of oscillations slowly increases if we go from $\xi_y = 0$ towards the QPT line $\xi_y = 2.06$. It has a finite value at the QPT, i.e., in the limit $\xi_y \rightarrow \sqrt{1 + \Omega_x^2}/2$, $\partial C_s(t)/\partial \xi_y \rightarrow 2t^2 \sqrt{1 + \Omega_x^2}$, which indicates that the behaviour of the NC in the symmetric phase is regular. When we approach the QPT line, it remains analytical. In contrast, in the broken-symmetry phase, the derivative of the NC, $\partial C_b(t)/\partial \xi_y$ diverges at the QPT, showing the non-analytical nature of the NC at these points. Furthermore, there is still sinusoidal motion in this phase, but the amplitude of the oscillations gradually decreases and decays to zero as we move far away from the QPT. In conclusion, the complexity of the FOTOC operator in the broken-symmetry phase captures information about QPTs, whereas this is not the case if one approaches the QPT from the symmetric phase. Although, both the phases resemble Hamiltonians of the harmonic oscillator, the difference comes from the presence of cross terms in \hat{Q} and \hat{P} in the broken-symmetry phase. Indeed, we may remove these cross terms by linear canonical transformations, but then this procedure will involve change of the basis of the system (from $\{\hat{Q}, \hat{P}\}$ to $\{\hat{Q}', \hat{P}'\}$) and the comparison of the NC in the two phases will lose meaning. What we have established here is the fact that in terms of the original $\{\hat{Q}, \hat{P}\}$ coordinates, the NC serves as a diagnostic tool for the QPT in the broken-symmetry phase.

At this point, it is important to note that the universal relation between complexity and the thermal OTOC, complexity = $-\log(\text{OTOC})$, mentioned in [35, 36] does not hold with the FOTOC, as we have checked all the regions of the parameter space, including unstable points and QPTs. The reason for this is clear from the construction of the FOTOC operator, where we chose \hat{V} as the projection operator rather than the time-independent FOTOC operator found in thermal and microcanonical OTOCs. As a result, we cannot establish any relationship between the FOTOC and complexity using the FOTOC operator.

V. GEOMETRY OF QUASI-SCRAMBLED EXCITED STATE

The geometry of the ground and excited states of an eLMG model was studied in [28], where the QIM and the corresponding Ricci scalar in the parameter space (Ω_x, ξ_y) was computed in the thermodynamic limit. The Ricci scalar turned out to be constant in the symmetric phases of both these states, even though a singularity appeared in all the metric components at the QPT, i.e., $\xi_y = -\sqrt{1 + \Omega_x^2}/2$ for the ground state, and $\xi_y = \sqrt{1 + \Omega_x^2}/2$ for the excited state although these are coordinate singularities, and not genuine curvature singularities. Furthermore, the Ricci scalar was found to be

always negative, implying that the ground and excited state geometries are hyperbolic.

Now we show that the situation qualitatively changes if we introduce a weak perturbation in the ground and excited states. The ground state analysis is summarised in Appendix B. The wavefunction of the excited state after a perturbation takes the form:

$$|\Psi(t)\rangle_{s,b} = e^{i\hat{H}_{s,b}t} e^{i\varepsilon\hat{Q}} e^{-i\hat{H}_{s,b}t} |0\rangle_{s,b} \equiv e^{i\varepsilon\hat{Q}_{s,b}(t)} |0\rangle_{s,b}, \quad (21)$$

where $\hat{Q}_{s,b}$ was computed in the section IV, $\hat{H}_{s,b}$ is given by Eq. (15) and (16), and $|0\rangle_{s,b}$ is the excited state of the symmetric and broken-symmetry phases, with frequencies ω_s and ω_b , respectively. Note that Eq. (9) is only the intermediate transformation for \hat{Q} and \hat{P} . The general transformation, which will cast the Hamiltonians $\hat{H}_{s,b}$ into that of a harmonic oscillator is given by

$$\begin{aligned} \hat{Q} &= \left(\frac{\Gamma_-}{4\sqrt{1+\Omega_x^2}} \right)^{1/4} (\gamma_s^\dagger + \gamma_s), \\ \hat{P} &= i \left(\frac{\sqrt{1+\Omega_x^2}}{4\Gamma_-} \right)^{1/4} (\gamma_s^\dagger - \gamma_s), \end{aligned} \quad (22)$$

for the symmetric phase, and $\hat{Q} = \sqrt{(\xi_y\omega_b)/(4\xi_y^2-1)}(\gamma_b^\dagger + \gamma_b)$, $\hat{P} = \mathcal{V}\gamma_b^\dagger + \mathcal{V}^*\gamma_b$, for the broken-symmetry phase, where

$$\mathcal{V} = \frac{\Omega_x}{\sqrt{4\xi_y\omega_b(4\xi_y^2-1)}} + i\sqrt{\frac{4\xi_y^2-1}{4\xi_y\omega_b}}. \quad (23)$$

Here, \mathcal{V}^* denotes the complex conjugate of \mathcal{V} , and $\gamma_{s,b}^\dagger$ and $\gamma_{s,b}$ are the Bogoliubov creation and annihilation operators respectively, such that $\gamma_{s,b}|0\rangle_{s,b} = 0$. In [45, 46], a nice physical interpretation of the perturbed state of the form Eq. (21) was given: we first prepare the excited state at time $t = 0$, and then, at a later time t , we apply a suitably small perturbation, i.e., a FOTOC operator, to obtain the perturbed excited state. Eq. (21) can now be read straightforwardly as follows: for a given excited state, the operator $e^{-i\hat{H}_{s,b}t}$ acts trivially on that state. Then, the FOTOC operator is a kind of displacement operator that shifts the state by momentum ε in phase space. Finally, we perform the reverse time evolution, which typically results in a state's rotation about the origin of the phase space. Fig. (4) depicts a visual representation of these phase space distributions, with the ground state characterised by an uncertainty bubble. The graphic clearly shows that the distribution remains confined, but has traveled around in phase space, a phenomenon referred to in the current literature as quasi-scrambling [26].

As mentioned in the introduction, there are two distinct types of scramblings: genuine scrambling, in which

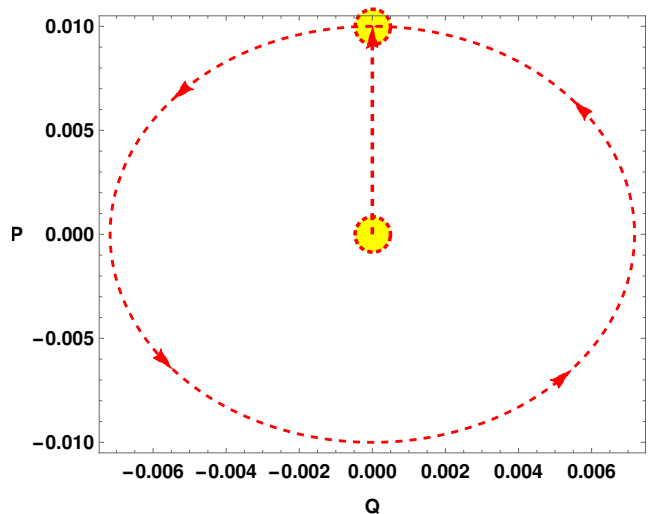


FIG. 4: Phase space distribution of the FOTOC operator with $\Omega_x = 4$, $\xi_y = 1$, and $\varepsilon = 0.01$. The dotted circle represents the quantum uncertainty of the ground state, which moves around in phase space with time, as shown by dotted lines and arrows. The distribution (uncertainty bubble) remains localized under Gaussian dynamics $\hat{H}_{s,b}$, depicting quasi-scrambling.

the distribution of operators spreads widely throughout the phase space, and quasi-scrambling, in which the distribution stays localised but is mobile in phase space. One of the key distinctions between quasi-scrambling and genuine scrambling is whether the time evolution is generated by Gaussian or non-Gaussian unitaries. Gaussian dynamics does not have the ability to spread an operator distribution in phase space, and we identify its dynamics as quasi-scrambling. On the other hand, in non-Gaussian dynamics, an operator distribution spreads significantly over phase space, and thus non-Gaussian dynamics give genuine scrambling. In Eq. (21), the temporal evolution is performed by Gaussian unitaries generated by the Hamiltonians $\hat{H}_{s,b}$. So, the perturbed state $|\Psi(t)\rangle_{s,b}$ is a state after the information has been quasi-scrambled, and we will now study the geometry of this quasi-scrambled state.

Following [40–43], the QIM g_{ij} is the real (symmetric) part of quantum geometric tensor denoted by χ_{ij} takes the form

$$\chi_{ij} = \sum_{m \neq n} \frac{\langle n | \partial_i \hat{H} | m \rangle \langle m | \partial_j \hat{H} | n \rangle}{(E_m - E_n)^2}, \quad (24)$$

where E_n is the non-degenerate eigenvalue corresponding to the orthonormal eigenvector $|n\rangle$ of the system whose Hamiltonian is \hat{H} . To study the geometry of the perturbed state, we first rewrite it in a simpler form using Bogoliubov operators $\gamma_{s,b}$, and further using the Baker-

Campbell-Hausdorff formula, we obtain

$$|\Psi(t)\rangle_{s,b} = \sum_{l=0}^{\infty} e^{-\frac{\varepsilon^2}{2} |\mathcal{B}_{s,b}(t)|^2} \frac{(i\varepsilon \mathcal{B}_{s,b}(t))^l}{\sqrt{l!}} |l\rangle_{s,b}, \quad (25)$$

where we have defined

$$\begin{aligned} \mathcal{B}_s(t) &= \left(\frac{\Gamma_-}{4\sqrt{1+\Omega_x^2}} \right)^{1/4} \mathcal{F}_s(t) + i \left(\frac{\sqrt{1+\Omega_x^2}}{4\Gamma_-} \right)^{1/4} \mathcal{G}_s(t), \\ \mathcal{B}_b(t) &= \sqrt{\frac{\xi_y \omega_b}{4\xi_y^2 - 1}} \mathcal{F}_b(t) + \mathcal{V} \mathcal{G}_b(t), \end{aligned} \quad (26)$$

and $|l\rangle_{s,b}$ are the eigenstates of $\gamma_{s,b}$. We can expand

$$|\Psi(t)\rangle_{s,b} = |0\rangle_{s,b} + i\varepsilon \mathcal{B}_{s,b}(t) |1\rangle_{s,b} + \mathcal{O}(\varepsilon^2), \quad (27)$$

since ε is a small number, which we will choose to be $\varepsilon = 0.01$ in the analysis to follow. The QIM for the state $|0\rangle_{s,b}$ has been computed in [28], and we list the additional terms, proportional to ε in the symmetric phase,

$$\begin{aligned} g_{\Omega_x \Omega_x} &= \varepsilon \frac{\sqrt{j} \Omega_x t \left(2\xi_y^2 - 3\xi_y \sqrt{1+\Omega_x^2} + 1 + \Omega_x^2 \right) \cos \omega_s t}{(1 + \Omega_x^2)^{7/4} \Gamma_-^{3/2}}, \\ g_{\Omega_x \xi_y} &= -\varepsilon \frac{\sqrt{j} t \cos \omega_s t}{2(1 + \Omega_x^2)^{3/4} \Gamma_-^{1/2}}, \quad g_{\Omega_x t} = \varepsilon \frac{\sqrt{j} \Gamma_-^{1/2} \cos \omega_s t}{2(1 + \Omega_x^2)^{3/4}}, \\ g_{\xi_y \xi_y} &= g_{\xi_y t} = g_{tt} = 0, \end{aligned} \quad (28)$$

where $\mathcal{O}(1/j)$ terms are neglected. It becomes cumbersome

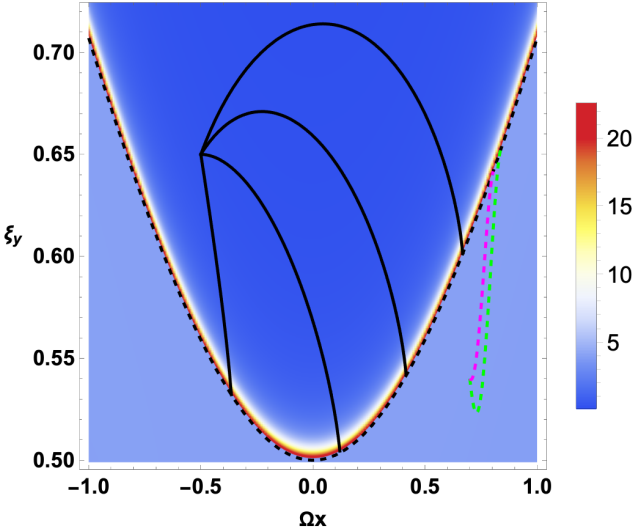


FIG. 5: The Ricci scalar of the geometry of the quasi-scrambled state, for $t = 4$, $j = 100$. The dashed black line separates the two phases. The solid black, the green and the magenta lines are plots of geodesics, see the main text.

some to present the equations of the metric components

in the broken-symmetry phase, and we omit these for brevity.

Our main results are shown graphically in Fig. (5), where the background depicts the Ricci scalar in the two phases separated by the dashed black line. In the broken-symmetry phase $\xi_y > 1/2\sqrt{1+\Omega_x^2}$, this diverges at the phase transition, and we find that this divergence is absent if we approach the phase transition from the symmetric phase. Here, for illustration, we have taken $t = 4$ and $j = 100$, with $\varepsilon = 0.01$ as mentioned before. We also plot a few typical geodesics for the geometries, by numerically solving the geodesic equation

$$\frac{d^2 x^i}{d\tau^2} + \Gamma_{jl}^i \frac{dx^j}{d\tau} \frac{dx^l}{d\tau} = 0, \quad (29)$$

with Γ_{jl}^i being the Christoffel connections, and $x^i = (\Omega_x(\tau), \xi_y(\tau))$, and we use the normalisation condition $g_{ij} \dot{x}^i \dot{x}^j = 1$. Here τ is an affine parameter along the geodesic and the overdot indicates a differentiation with respect to τ . In the broken-symmetry phase, we start the geodesics from $(\Omega_x, \xi_y) = (-0.5, 0.65)$ with the initial value of $\dot{\xi}_y = -0.08, 0, 0.02$ and 0.03 for the solid black lines from bottom to top, respectively, and the initial value of $\dot{\Omega}_x$ is determined from the normalisation condition. In the symmetric phase, the dashed green and magenta lines correspond to the initial value of $(\Omega_x, \xi_y) = (0.7, 0.54)$ with the initial value of $\dot{\xi}_y = -0.12$ and -0.02 , respectively.

In the symmetric phase, our results indicate that $R \rightarrow -4$ as $\xi_y \rightarrow 1/2\sqrt{1+\Omega_x^2}$. Away from this phase transition line, the dependence of R with Ω_x and ξ_y does not show any interesting behaviour. We also computed the Fubini-Study complexity (defined as the geodesic length) by numerically inverting the solution of the geodesic equation [40–43]. It can be seen from Fig. (5) that in both phases, the geodesics are “attracted” towards the phase boundary and ends there, and these do not show any particularly interesting behaviour.

VI. CONCLUSIONS

In this work, we have demonstrated how FOTOCs have distinctive behaviour at QPTs in the ground and excited states. We have illustrated this by analysing the dynamics of the FOTOC in two phases of an eLMG model. We have also established the connection between the FOTOC and the Loschmidt echo at small times, by a suitable time-rescaling. Next, we computed the NC of the FOTOC operator and showed that its derivative is divergent as one approaches QPT from the broken-symmetry phase side. Also, the geometry of the parameter space of this model was studied by perturbing the ground and excited states with the FOTOC operator. These states are quasi-scrambled states after the perturbation, and analytic computations were performed to extract the QIM.

This yields a diverging Ricci scalar at QPTs from the broken-symmetry phase side, in contrast to the unperturbed states whose Ricci scalar does not possess any such feature.

Our study focussed only on the eLMG model, whose Hamiltonian reduces to that of a harmonic oscillator : a Gaussian unitary. The time-evolution generated by a Gaussian unitary will give quasi-scrambling. It will be interesting to explore the QIG with non-Gaussian unitaries that offer genuine scrambling. We leave this for a future work.

Appendix A

In this section, we present a detailed calculation of the NC following [35]. We apply Nielsen's geometric approach to find the optimal circuit. The first step is to parametrize the unitary as a path-ordered exponential

$$U(\tau) = \overleftarrow{\mathcal{P}} \exp \left(\int_0^\tau d\tau' H(\tau') \right), \quad (\text{A1})$$

with $H(\tau') = \sum_{I \in \{1,3\}} Y^I(\tau') M_I$, $Y^I(\tau')$ are control functions and specifies a particular circuit in the space of unitaries, and M_I are the three-dimensional representation of the Heisenberg group generators

$$M_1 = \begin{bmatrix} 0 & 1 & 0 \\ 0 & 0 & 0 \\ 0 & 0 & 0 \end{bmatrix}, \quad M_2 = \begin{bmatrix} 0 & 0 & 0 \\ 0 & 0 & 1 \\ 0 & 0 & 0 \end{bmatrix}, \quad M_3 = \begin{bmatrix} 0 & 0 & 1 \\ 0 & 0 & 0 \\ 0 & 0 & 0 \end{bmatrix}, \quad (\text{A2})$$

satisfying the Heisenberg algebra. The explicit form of the functions $Y^I(\tau)$ can be evaluated by using Eq. (A1) and the expressions of M_I ,

$$Y^I(\tau) = -\text{Tr} \left[(\partial_\tau U(\tau)) U^{-1}(\tau) M_I^T \right]. \quad (\text{A3})$$

By following the usual procedure [37], we can define the cost functional for various paths

$$\mathcal{D}[U(\tau)] = \int_0^1 d\tau' \sum_I |Y^I(\tau')|^2, \quad (\text{A4})$$

where we followed $\kappa = 2$ cost functions. Note that the $\kappa = 2$ cost function and the F_2 cost function will provide the exact same extremal trajectories or optimal circuits [39]. The minimal value of the above cost functional will give the required complexity, and it can be obtained by evaluating it on the geodesics of unitary space with the boundary conditions

$$\tau = 0, U(\tau = 0) = \mathbb{1}, \quad \tau = 1, U(\tau = 1) = \hat{W}_{s,b}(t). \quad (\text{A5})$$

We first represent the FOTOC operator in Heisenberg group generators as $e^{\varepsilon(\mathcal{F}_{s,b}(t)M_1 + \mathcal{G}_{s,b}(t)M_2)}$, which is solved as,

$$\hat{W}_{s,b}(t) = \begin{bmatrix} 1 & \varepsilon\mathcal{F}_{s,b}(t) & \frac{\varepsilon^2}{2}\mathcal{F}_{s,b}(t)\mathcal{G}_{s,b}(t) \\ 0 & 1 & \varepsilon\mathcal{G}_{s,b}(t) \\ 0 & 0 & 1 \end{bmatrix}. \quad (\text{A6})$$

In general, we can parametrize an element of Heisenberg group by $U(\tau)$ where,

$$U(\tau) = \begin{bmatrix} 1 & x_1(\tau) & x_3(\tau) \\ 0 & 1 & x_2(\tau) \\ 0 & 0 & 1 \end{bmatrix}, \quad (\text{A7})$$

then the Eq. (A4) can be written in the form:

$$\mathcal{D}[U(\tau)] = \int_0^1 d\tau \left((1 + x_2^2) \left(\frac{dx_1}{d\tau} \right)^2 + \left(\frac{dx_2}{d\tau} \right)^2 + \left(\frac{dx_3}{d\tau} \right)^2 - 2x_2 \left(\frac{dx_1}{d\tau} \right) \left(\frac{dx_3}{d\tau} \right) \right). \quad (\text{A8})$$

The geodesic equations corresponding to the above metric are

$$\begin{aligned} \dot{x}_2(x_2\dot{x}_1 - \dot{x}_3) + \ddot{x}_1 &= 0, & \dot{x}_1(-x_2\dot{x}_1 - \dot{x}_3) + \ddot{x}_2 &= 0, \\ \dot{x}_2((x_2^2 - 1)\dot{x}_1 - x_2\dot{x}_3) + \ddot{x}_3 &= 0, \end{aligned} \quad (\text{A9})$$

where the dot represents the derivative with respect to τ , and is solved using above boundary conditions to get

$$\begin{aligned} x_1(\tau) &= \varepsilon\mathcal{F}_{s,b}(t)\tau, & x_2(\tau) &= \varepsilon\mathcal{G}_{s,b}(t)\tau, \\ x_3(\tau) &= \frac{\varepsilon^2}{2}\mathcal{F}_{s,b}(t)\mathcal{G}_{s,b}(t)\tau^2. \end{aligned} \quad (\text{A10})$$

Using the above solution in Eq. (A8), the final expression for the NC is

$$\mathcal{C}_{s,b}(t) = \varepsilon^2 (\mathcal{F}_{s,b}^2(t) + \mathcal{G}_{s,b}^2(t)). \quad (\text{A11})$$

Appendix B

In this section, for the sake of completeness, we evaluate the metric components of the perturbed ground state. The Hamiltonian of the ground state takes the form:

$$\hat{H}_g \simeq -j\sqrt{1 + \Omega_x^2} + \left(\frac{\sqrt{1 + \Omega_x^2} + 2\xi_y}{2} \right) \hat{P}^2 + \frac{\sqrt{1 + \Omega_x^2}}{2} \hat{Q}^2, \quad (\text{B1})$$

which describes the harmonic oscillator with frequency $\omega_g = (1 + \Omega_x^2)^{1/4} \sqrt{\Gamma_+}$ and $\Gamma_+ = \sqrt{1 + \Omega_x^2} + 2\xi_y$. The Bogoliubov transformation of the ground state is

$$\begin{aligned} \hat{Q} &= \left(\frac{\Gamma_+}{4\sqrt{1 + \Omega_x^2}} \right)^{1/4} (\gamma_g^\dagger + \gamma_g), \\ \hat{P} &= i \left(\frac{\sqrt{1 + \Omega_x^2}}{4\Gamma_+} \right)^{1/4} (\gamma_g^\dagger - \gamma_g), \end{aligned} \quad (\text{B2})$$

with $\gamma_g |0\rangle_g = 0$ and $|0\rangle_g$ is the Bogoliubov ground state. Following a similar analysis as for the excited state, we perturb the ground state as

$$|\Psi(t)\rangle_g = e^{i\hat{H}_g t} e^{i\varepsilon\hat{Q}} e^{-i\hat{H}_g t} |0\rangle_g \equiv e^{i\varepsilon\hat{Q}_g(t)} |0\rangle_g, \quad (\text{B3})$$

with

$$\hat{Q}_g = \hat{Q} \cos \omega_g t + \hat{P} \frac{\Gamma_+^{1/2} \sin \omega_g t}{(1 + \Omega_x^2)^{1/4}}, \quad (\text{B4})$$

and the metric components proportional to ε turn out to be

$$\begin{aligned} g_{\Omega_x \Omega_x} &= \varepsilon \frac{\sqrt{j} \Omega_x t \left(2\xi_y^2 + 3\xi_y \sqrt{1 + \Omega_x^2} + 1 + \Omega_x^2 \right) \cos \omega_g t}{(1 + \Omega_x^2)^{7/4} \Gamma_+^{3/2}} \\ &\quad - \varepsilon \frac{\sqrt{j} \Omega_x \xi_y \sin \omega_g t}{(1 + \Omega_x^2)^2 \Gamma_+}, \\ g_{\Omega_x \xi_y} &= \varepsilon \frac{\sqrt{j} t \cos \omega_g t}{2(1 + \Omega_x^2)^{3/4} \Gamma_+^{1/2}} + \varepsilon \frac{\sqrt{j} \sin \omega_g t}{2(1 + \Omega_x^2) \Gamma_+}, \\ g_{\Omega_x t} &= \varepsilon \frac{\sqrt{j} \Gamma_+^{1/2} \cos \omega_g t}{2(1 + \Omega_x^2)^{3/4}}, \quad g_{\xi_y \xi_y} = g_{\xi_y t} = g_{tt} = 0. \quad (\text{B5}) \end{aligned}$$

We have computed the Ricci scalar in the parameter space (Ω_x, ξ_y) for fixed t and find that $R \rightarrow -4$ as $\xi_y \rightarrow -1/2\sqrt{1 + \Omega_x^2}$ similar to the situation in the symmetric phase.

-
- [1] A. Larkin and Yu. N. Ovchinnikov, *Sov. Phys. JETP* **28**, 1200 (1969).
- [2] J. Chavez-Carlos, B. Lopez-del-Carpio, M. A. Bastarrachea-Magnani, P. Stransky, S. Lerma-Hernandez, L. F. Santos, and J. G. Hirsch, *Phys. Rev. Lett.* **122**, 024101 (2019).
- [3] T. Akutagawa, K. Hashimoto, T. Sasaki, and R. Watanabe, *J. High Energy Phys.* 08 (2020) 013.
- [4] K. Hashimoto, K. Murata, and R. Yoshii, *J. High Energy Phys.* 10 (2017) 138.
- [5] E. B. Rozenbaum, S. Ganeshan, and V. Galitski, *Phys. Rev. Lett.* **118**, 086801 (2017).
- [6] B. Swingle, G. Bentsen, M. Schleier-Smith, and P. Hayden, *Phys. Rev. A* **94**, 040302(R) (2016).
- [7] M. Garttner, P. Hauke, and A. M. Rey, *Phys. Rev. Lett.* **120**, 040402 (2018).
- [8] A. W. Harrow, L. Kong, Z. W. Liu, S. Mehraban, and P. W. Shor, *Phys. Rev. X Quantum* **2**, 020339 (2021).
- [9] H. Shen, P. Zhang, R. Fan, and H. Zhai, *Phys. Rev. B* **96**, 054503 (2017).
- [10] Q. Wang, and F. P. Bernal, *Phys. Rev. A* **100**, 062113 (2019).
- [11] R. A. Kidd, A. Safavi-Naini, and J. F. Corney, *Phys. Rev. A* **102**, 023330 (2020).
- [12] M. Heyl, F. Pollmann, and B. Dora, *Phys. Rev. Lett.* **121**, 016801, (2018).
- [13] R. K. Shukla, G. K. Naik, and S. K. Mishra, *Europhys. Lett.* **132**, 47003 (2021)
- [14] K. B. Huh, K. Ikeda, V. Jahnke, and K. Y. Kim, *Phys. Rev. E* **104**, 024136 (2021).
- [15] J. Khalouf-Rivera, J. Gamito, F. Perez-Bernal, J. M. Arias, P. Perez-Fernandez, arXiv:2207.04489 [quant-ph].
- [16] S. Pilatowsky-Cameo, J. Chavez-Carlos, M. A. Bastarrachea-Magnani, P. Stranský, S. Lerma-Hernandez, L. F. Santos, and J. G. Hirsch, *Phys. Rev. E* **101**, 010202(R) (2020).
- [17] R. J. Lewis-Swan, A. Safavi-Naini, J. J. Bollinger, and A. M. Rey, *Nat. Commun.* **10**, 1581 (2019).
- [18] A. Safavi-Naini, R. J. Lewis-Swan, J. G. Bohnet, M. Garttner, K. A. Gilmore, J. E. Jordan, J. Cohn, J. K. Freericks, A. M. Rey, and J. J. Bollinger, *Phys. Rev. Lett.* **121**, 040503 (2018).
- [19] M. K. Joshi, A. Elben, B. Vermersch, T. Brydges, C. Maier, P. Zoller, R. Blatt, and C. F. Roos, *Phys. Rev. Lett.* **124**, 240505 (2020).
- [20] A. M. Green, A. Elben, C. H. Alderete, L. K. Joshi, N. H. Nguyen, T. V. Zache, Y. Zhu, B. Sundar, and N. M. Linke, *Phys. Rev. Lett.* **128**, 140601 (2022).
- [21] K. A. Landsman, C. Figgatt, T. Schuster, N. M. Linke, B. Yoshida, N. Y. Yao, and C. Monroe, *Nature (London)* **567**, 61 (2019).
- [22] M. Garttner, et al., *Nat. Phys.* **13**, 781-786 (2017).
- [23] B. Swingle, *Nat. Phys.* **14**, 988 (2018).
- [24] X. Mi et al., arXiv:2101.08870 [quant-ph].
- [25] S. Xu, and B. Swingle, arXiv:2202.07060 [quant-ph].
- [26] Q. Zhuang, T. Schuster, B. Yoshida, and N. Y. Yao, *Phys. Rev. A* **99**, 062334 (2019).
- [27] B. Yan, L. Cincio, and W. H. Zurek, *Phys. Rev. Lett.* **124**, 160603 (2020).
- [28] D. Gutierrez-Ruiz, D. Gonzalez, J. Chavez-Carlos, J. Hirsch, J. D. Vergara, *Phys. Rev. B* **103**, 174104 (2021).
- [29] H. J. Lipkin, N. Meshkov, and A. J. Glick, *Nucl. Phys.* **62**, 188 (1965).
- [30] R. Botet, R. Jullien, P. Pfeuty, *Phys. Rev. Lett.* **49**, 478 (1982).
- [31] R. Botet, R. Jullien, *Phys. Rev. B* **28**, 3955 (1982).
- [32] A. Dey, S. Mahapatra, P. Roy, and T. Sarkar, *Phys. Rev. E* **86**, 031137 (2012).
- [33] L. C. Qu, J. Chen, and Y. X. Liu, *Phys. Rev. D* **105**, 126015 (2022).
- [34] T. Ali, A. Bhattacharyya, S. S. Haque, E. H. Kim, N. Moynihan, and J. Murugan, *Phys. Rev. D* **101**, 026021 (2020).

- [35] A. Bhattacharyya, W. Chemissany, S. S. Haque, J. Murugan, and B. Yan, *SciPost Phys. Core* **4**, 002 (2021).
- [36] S. Choudhury, A. Dutta, and D. Ray, *J. High Energy Phys.* 04 (2021) 138.
- [37] F. Liu, S. Whitsitt, J. B. Curtis, R. Lundgren, P. Titum, Z. C. Yang, J. R. Garrison, and A. V. Gorshkov, *Phys. Rev. Res.* **2**, 013323 (2020).
- [38] S. S. Haque, C. Jana, B. Underwood, arXiv:2110:08356 [hep-th].
- [39] M. Guo, J. Hernandez, R. C. Myers, and S.-M. Ruan, *J. High Energy Phys.* 10 (2018) 011.
- [40] N. Jaiswal, M. Gautam, and T. Sarkar, *Phys. Rev. E* **104**, 024127 (2021).
- [41] N. Jaiswal, M. Gautam, and T. Sarkar, *J. Stat. Mech.* (2022), 073105.
- [42] M. Gautam, N. Jaiswal, A. Gill, and T. Sarkar, arXiv:2207.14090 [quant-ph].
- [43] K. Pal, K. Pal, and T. Sarkar, arXiv:2204.06354 [quant-ph].
- [44] M. Miyaji, *J. High Energy Phys.* 09 (2016) 002.
- [45] S. H. Shenker and D. Stanford, *J. High Energy Phys.* 03 (2014) 067.
- [46] D. A. Roberts, D. Stanford, and L. Susskind, *J. High Energy Phys.* 03 (2015) 051.
- [47] S. Hawking, *Nucl. Phys. B* **144**, 349 (1978).